Biochimica et Biophysica Acta 1850 (2015) 329–342

Contents lists available at ScienceDirect

Biochimica et Biophysica Acta

journal homepage: www.elsevier.com/locate/bbagen

Interaction of human telomeric G-quadruplex DNA with thymoquinone: A possible mechanism for thymoquinone anticancer effect

Alaa A. Salem [a,*], Ismail A. El Haty [a], Ibrahim M. Abdou [a], Yuguang Mu [b]

[a] Department of Chemistry, College of Science, United Arab Emirates University, P.O. Box 15551, Al Ain, United Arab Emirates
[b] School of Biological Sciences, College of Science, Nanyang Technological University, Singapore 637551, Singapore

ARTICLE INFO

Article history:
Received 27 July 2014
Received in revised form 16 October 2014
Accepted 20 October 2014
Available online 24 October 2014

Keywords:
Human telomere
DNA
G-quadruplex
Thymoquinone
Anticancer
Calf thymus DNA

ABSTRACT

Background: Thymoquinone (TQ) has been documented to possess chemo-preventive and chemotherapeutic antitumor effects. Studies reported that TQ inhibits the growth of cancer cells in animal models, culture and xenografted tumors. Molecular mechanisms underlying these anticancer effects were attributed to inductions of cell cycle arrest, apoptosis, oxidative damage of cellular macromolecules, blockade of tumor angiogenesis and inhibitions in migration, invasion and metastasis of cancer cells.
On the other hand, human telomere DNA plays a role in regulating genes' transcriptions. It folds up into G-quadruplex structures that inhibit telomerase enzyme over-expressed in cancerous cells. Molecules that selectively stabilize G-quadruplex are potential anticancer agents. Therefore, this work aimed to explore the interaction of TQ with G-quadruplex DNA as a possible underlying mechanism for the anticancer effect of TQ.
Methods: Interactions of TQ with telomeric G-quadruplex (5′-AGGG(TTAGGG)$_3$-3′) and duplex DNAs were studied using UV–vis, fluorescence, circular dichroism, liquid and solid NMR (^{1}H and ^{13}C), melting temperature and docking simulation.
Results: Changes in UV–vis, CD, fluorescence, ^{1}H NMR and ^{13}C NMR, spectra as well as melting temperatures and docking simulations provided evidences for TQ's interactions with G-quadruplex. TQ was found to interact with G-quadruplex on two binding sites adjacent to the TTA loop with binding constants 1.80×10^5 and 1.12×10^7 M^{-1}. Melting temperatures indicated that TQ stabilized G-quadruplex by 5.6 °C and destabilized ct-DNA by 5.1 °C. Selectivity experiment indicated that TQ is preferentially binding to G-quadruplex over duplex with selectivity coefficients of 2.80–3.33 $\times 10^{-3}$. Results suggested an intercalation binding mode based on π–π stacking.
Conclusion: Our results propose that TQ can possibly act as a G-quadruplex DNA stabilizer and subsequently contribute to the inhibition of telomerase enzyme and cancer's proliferation.
General significance: Our results represent a change in the paradigms reported for structural features of G-quadruplex's stabilizers and anticancer mechanisms of TQ.

1. Introduction

Nigella sativa or black seed has been used for treating several diseases over centuries. Thymoquinone, 2-isopropyl-5-methylbenzo-1,4-quinone; is the major constituent (30–48%) of the seeds' essential oil [1] (Scheme 1). TQ is of low general toxicity and has shown antitumor effects in numerous cancer culture cell lines and animal models [2,3]. Other pleiotropic pharmacological effects of TQ include antioxidant, anti-inflammatory, antidiabetic, free radical scavenger, modulator for anti-oxidant enzymes, inhibitor for the pro-inflammatory transcription factors and inflammatory cytokine growth mediators as well as affecting autoimmune diseases [1].

Numerous in-vivo and in-vitro studies reported the anti-cancer and chemo-preventive effects of TQ against different malignancies [2]. The works reported by Johnson and Worthen on the cytotoxic effects of TQ against human cancer cells initiated the growing interest in TQ as a potential chemopreventive agent [3,4]. Molecular targets of TQ as a preventive and chemotherapeutic anticancer agent have been discussed in a recent review by Kundu et al. They presented different molecular mechanisms associated with diverse biochemical processes underlying the anticancer effect of TQ [5]. TQ has shown to inhibit proliferation of neoplastic keratinocytes [6], glioma/glioblastoma (U87 MG and T98G, M059K and M059J) [7], breast adenocarcinoma (multi-drug-resistant MCF-7/TOPO, MCF-7, MDA-MB-231 and BT-474) [8,9], leukemia (HL-60 and Jurkat) [10], lung cancer (NCI-H460 and A549) [11,12], colorectal carcinoma (HT-29, HCT-116, DLD-1, Lovo and Caco-2) [13], pancreatic cancer (MIA PaCa-2, HPAC and BxPC-3) [12], osteosarcoma

* Corresponding author. Tel.: +971 37136120.
E-mail address: asalem@uaeu.ac.ae (A.A. Salem).

http://dx.doi.org/10.1016/j.bbagen.2014.10.018
0304-4165/

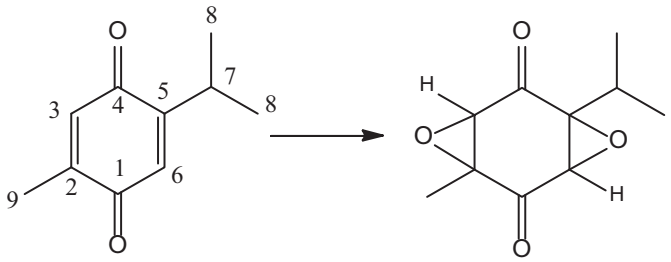

Scheme 1. Conversion of TQ to di-peroxy TQ.

(MG63 and MNNG/HOS) [14], and prostate cancer (LNCaP, C4-2B, DU145 and PC-3) [15].

TQ was also shown to induce G2/M arrest, inactivate PI3K/Akt and nuclear factor–kB pathways in human cholangiocarcinomas both in-vitro and in-vivo [16]. Hamid et al. indicated that TQ targets specific genes in the estrogen metabolic and interferon pathways in MCF7 breast cancer cells [17]. TQ's molecular mechanisms based on cell cycle arrest were reported. Cell cycle arrests in SP-1 mouse papilloma and HCT116 human colorectal carcinoma cells were attributed to increase in p16 expression and decrease in cyclin D1 or regulation of p53 [6,18]. Cell cycle arrests were attributed to inhibition of G1 progression in prostate cancer cells, increasing the p53 and p21 proteins in MNNG/HOS human osteosarcoma cells and to increasing MCF-7/DOX doxorubicin-resistant in breast cancer cells [15,19].

The apoptotic effect of TQ in HCT116 human colorectal carcinoma cells was attributed to interfering the p53-dependent and independent pathways [18,20] and to blockage of JAK2- and Src-mediated phosphorylation of EGF receptor tyrosine kinase [21]. Apoptosis in p53-null myeloblastic leukemia HL-60 cells was attributed to the activation of caspases 8, 9 and 3, and the increase of the Bax/Bcl-2 ratio [22]. TQ also showed to cause apoptosis in PC-3 prostate cancer cells [15] and in U266 multiple myeloma cells [23]. Sethi et al. reported that TQ suppresses the TNF-induced NF-kB-regulated gene products that include IAP1, IAP2, XIAP, Bcl-2, Bcl-xL, survivin, COX-2, cyclin D1, c-Myc, MMP-9 and VEGF, in KBM-5 human myeloid cells [24]. Apoptosis mechanisms based on down regulating Mucin-4 expressed during the proteasomal pathway in FG/COLO357 pancreatic cancer cells and inhibition of Akt activation and increasing Bax/Bcl-2 ratio in primary effusion lymphoma cells were also reported [25,26].

In comparison to cisplatin, TQ was found to be more potent on SiHa human cervical squamous carcinoma cells [27]. It also inhibited tumor engrafted cells types HCT116 and PC-3 prostate cancer in mice and inhibits invasions of MDA-MB-231 and C26 breast and colon cancers [28,9]. Reasons were attributed to angiogenesis inhibitions in migration, invasion and/or tube formation of human umbilical vein endothelial cells, FG/COLO357 cells and of NCI-H460 cells [29].

Other mechanisms based on activating JNK's phosphorylation in PC-3 prostate cancer cells [15], activating peroxisome proliferator-activated receptors (PPARs) in MCF-7 breast cancer cells [9] and down-regulating cyclic nucleotide phosphodiesterases [30] were also reported. Gurung et al. have recently reported that TQ induces apoptosis and DNA's damage in human glioblastoma cells by oxidative damage of DNA which results in telomerase inhibition, telomere attrition and cell death [31].

On the other hand, identification of G-quadruplex structures in telomeric DNA and promoter regions of some oncogenes (e.g. *c-myc* and *c-kit*) has attracted the attentions of researchers over the last two decades to a hot topic strongly motivated by the desire to discover new anti-cancer drugs [32–35]. Folding telomeric DNA into G-quadruplex structures has shown to inhibit telomerase activity over expressed in cancer cells and subsequently control cells' transcriptions [36]. Molecules with high binding affinity towards G-quadruplex DNA structures may induce cell apoptosis, inhibit cancer proliferation and cause cancer relief. Thus, G-quadruplex stabilizers represent a potential avenue of compounds for developing effective anticancer therapeutic agents [37].

Several classes of compounds have been reported as G-quadruplex stabilizers, telomerase inhibitors and/or oncogene regulators. These included porphyrines [38], porphyrazines [39], phthalocyanines [40], cyclopyrroles [41], telomestatin [42] and porphyrin TMPyP4 [43] derivatives. The 5,10,15,20-tetra [4-hydroxyl-3-9-trimethyl-ammonium methyl-phenyl] showed higher selectivity due to the presence of four positively charged groups and four hydroxyl groups that can interact with the G-quadruplex loops and grooves [44]. In additions, acridines, acridones, perylene, corolone, anthraquinones and quinolone derivatives were reported to strongly interact with G-quadruplex by π–π stacking and with ds-DNA by intercalations or groove bindings between the duplex base pairs [32,45]. In the case of perylene, the length between the aromatic central core and the positively charged nitrogen atom of the lateral side chain as well as the basicity of the system was assumed responsible for giving rise better quadruplex stabilization [46,47]. Fonsecin B and methylene blue were reported as C-myc G-quadruplex stabilizers [48,49].

Porphyrin metal complexes with selenium, manganese (II), nickel (II) and copper (II) showed high binding affinities towards human telomeric and *c-myc* quadruplexes and inhibitions of their transcriptions [32,33]. Zinc (II) phthalocyanine [40], nickel (II) salphen [50], platinum (II) phenanthroline [51] and platinum dipyridophenazine [52] complexes were reported as having higher affinity and selectivity for quadruplex stabilization and telomerase inhibition. Iridium (III) complexes were used as G-quadruplex selective probe for the detections of gene deletion, base excision repair enzyme activity, cysteine and glutathione in aqueous solutions and T4 polynucleotide kinase activity [53].

The above studies indicated that molecules having a delocalized system to stack on the face of guanine quartet, a partial positive charge to intercalate in the center of the guanine quartet through interaction with electron pairs on carbonyl oxygens and/or positively charged substituents to interact with the grooves, loops or negatively charged phosphate backbones, can act as G-quadruplex stabilizers. Planar metal complexes with π-delocalized ligands and a strong electron withdrawing central metal ion were also assumed good stabilizers for G-quadruplex [54].

In spite of the growing literature on G-quadruplex's stabilizers, up to our knowledge, none of investigated molecules has passed to clinical trials due to their poor drug-like properties and/or selectivity. On contrary, the anticancer effects of TQ have been fully documented in literature. Several molecular mechanisms underlying these effects were proposed. However, TQ anticancer effects remained poorly understood [55]. Direct oxidative damage of DNA proposed by Gurung et al. was not supported by the low redox potential of TQ (+0.5928 V) compared to the redox potentials of guanine (+0.68 V) and adenine (+0.97 V) bases of DNA [31,56,57]. Subsequently an indirect oxidation mechanism might have been involved.

Therefore, this work aimed to investigate human telomere G-quadruplex DNA (5′-AGGG(TTAGGG)$_3$-3′) as a molecular target for TQ's anticancer effects. Evidences for the interaction of TQ with G-quadruplex and duplex DNAs were obtained using UV–vis, fluorescence, fluorescence quenching, circular dichroism and melting temperature curves. Binding sites were inferred using solid and liquid NMR as well as fluorescence quenching. Binding affinities were estimated using Scatchard plots. Stoichiometry and selectivity of TQ towards G-quadruplex over ds-DNA were also evaluated. Further evidences on binding sites and binding affinities were obtained using molecular docking. Up to our knowledge, interactions of small molecules such as TQ with G-quadruplex DNA have not been considered in literature.

2. Experimental

2.1. Materials and reagents

All chemicals were of the highest analytical purity available. TQ was purchased from Sigma-Aldrich (China). HPLC purified human telomere DNA with sequence 5′-AGGG(TTAGGG)$_3$-3′, complimentary strand 3′-TCCC(AATCCC)$_3$-5′ and fluorescein labeled 5′-Fl-AGGG(TTAGGG)$_3$-3′ were purchased from Alpha-DNA (Montreal, Canada). Calf thymus DNA (ct-DNA) extracted from male and female calf thymus tissues and consists of 41.9 mol% G–C and 58.1 mol% A–T linkages was purchased from Sigma-Aldrich (Germany). Its nominated molecular weight is (10–15) $\times$ 10^6 Da. Millipore deionized water was used throughout.

2.2. Apparatus

Absorption spectrophotometric measurements were carried out using RJ-45 diode array single beam UV–vis spectrophotometer matched with 1 cm quartz cells (Agilent Technologies, Austria). Fluorescence measurements were carried out using Cary Eclipse model-3 spectrofluorometer equipped with a high intensity Xenon flash lamp and 1.0 cm path length quartz cell (Varian, Austria). NMR measurements were made using Varian 400 MHz NMR (Varian, USA). CD measurements were made using Jasco J-815 spectrometer (Jasco, USA). The pH was measured using Orion-401-Plus pH meter supported with Orion glass electrode.

2.3. Standard solutions

2.3.1. Buffer solution

A Tris–KCl buffer solution, 0.01 M in Tris–hydroxymethyl-aminomethane, 0.001 M in EDTA and 0.1 M KCl, were prepared in deionized water using the standard procedure. The pH was adjusted to pH 7.4 using the glass electrode.

2.3.2. TQ solution

A 10^{-3} M TQ solution was prepared by dissolving 8.20 mg into 5.0 ml ethylene glycol. Resultant solution was made up to 50.0 ml using deionized water. Solutions having lower concentrations were prepared by appropriate dilution in Tris–KCl buffer.

2.3.3. DNA solutions

2.3.3.1. Human telomere DNA. Purchased synthetic ssDNA primers with human telomere sequence; 5′-AGGG(TTAGGG)$_3$-3′, fluorescein labeled primer Fl-5′-AGGG(TTAGGG)$_3$-3′ and complementary strand 3′-TCCC(AATCCC)$_3$-5′ were reconstituted by centrifugation for 3.0 min at 7000 rpm to collect DNA in the bottom of the tubes. A 2.0 ml Tris–KCl buffer was added to each tube and left for 2.0 min for rehydration. Solutions were vortexed for 30 s and reconstituted primers were kept overnight at 4 °C.

2.3.3.2. G-quadruplex DNA. G-quadruplex DNA was prepared by gently heating 1.0 ml of the stock telomere ssDNA solution up to 95 °C. Resultant solution was incubated for 10.0 min at 95 °C, left to cool at room temperature and then kept overnight at 4 °C in the fridge before use.

2.3.3.3. Hybridization of telomere DNA oligonucleotides. A 1×10^{-4} M telomere dsDNA was prepared by mixing equimolar amounts of 5′-AGGG(TTAGGG)$_3$-3′ (7.44×10^{-4} M) and its complementary strand 3′-TCCC (AA TCCC)$_3$-5′ (2.71×10^{-4} M). The solution was made up to 2.0 ml using Tris–KCl buffer pH 7.4, vortexed for 15 s, incubated for 10.0 min at 95 °C and left to cool to room temperature. Resultant hybridized dsDNA was kept in the fridge at 4 °C till use.

2.3.3.4. Calf thymus DNA. Calf thymus DNA (A 1000.0 μg/ml) was prepared by dissolving 10.0 mg into 10.0 ml Tris–KCl buffer without sonication or stirring. The solution was gently inverted overnight at 4 °C to prevent shearing and completely solubilize the large genomic DNA. Resultant ct-DNA solution is stable for more than 6 months at 4 °C in Tris–KCl buffer pH 7–8. Lower concentrations were prepared by accurate dilutions.

Concentrations of stock telomere ssDNA, fluorecine labeled DNA and ct-DNA solutions were determined by diluting 10.0 μl of each solution using Tris–KCl buffer (pH 7.4) to 1000.0 μl, vortexed for 15 s each and scanned for their absorbance at 260 and 280 nm. Concentrations in μg/ml were calculated using $C_{(\mu g/ml)} = A_{260} \times$ weight per OD $\times$ dilution factor, where OD is the optical density at 260 nm. The purity of oligonucleotides was estimated based on the A_{260}/A_{280} ratio. Ratios ≥ 1.8 were considered indicative for high purity of synthetic and ct-DNA.

2.4. Procedures

2.4.1. UV–vis titration of DNA

UV–vis titration was conducted by adding successive amounts of TQ (10.0 μl; 1×10^{-3} M) to 1.0 ml of G-quadruplex (1.44×10^{-6} M) or ct-DNA (50.00 μg/ml) in Tris–KCl buffer, pH 7.4. After each addition, solution was shacked, incubated for 3.0 min at room temperature and scanned in the range of 200–600 nm.

2.4.2. Circular dichroism titration

CD titrations were conducted by adding successive amounts of TQ (1×10^{-5} M) to 1.0 ml of G-quadruplex (3.6×10^{-6} M) or ct-DNA (50.00 μg/ml) in Tris–KCl-buffer, pH = 7.4. After each addition, the solution was shacked, incubated for 3 min at room temperature and scanned for its CD spectra in the range of 200–400 nm against blank. Spectra obtained were baseline corrected.

2.4.3. Fluorescence titrations

TQ was found to give fluorescence emission at λ_{max} of 330 nm using excitation λ_{max} of 295 nm. Therefore, fluorescence titration was conducted by adding successive portions (~10.00 μl) of G-quadruplex (1.44×10^{-4} M) or ct-DNA (1000 μg/ml) to 3.0 ml TQ (2×10^{-4} M or 5×10^{-5} M) in Tris–KCL-buffer. After each addition, the solution was stirred for 20 s, incubated for 3 min and scanned for emission spectra in the range of 300–500 nm using slit width of 10.00 nm. Titration stopped when no change in fluorescence intensity was observed.

Fluorescence quenching titration was done using fluorescein labeled G-quadruplex DNA (Fl-G-quadruplex) whose emission λ_{max} is 518 nm at excitation λ_{max} of 494 nm. The experiment was run by adding successive amounts of TQ (1×10^{-5} M) to 3.0 ml of Fl-G-quadruplex (1.99×10^{-6} M) in Tris–KCl-buffer, pH 7.4. After each addition, the solution was stirred for 20 s, incubated for 3 min and scanned for its emission spectra in the range of 500–700 nm using slit width of 5 nm.

2.4.4. Binding affinity

Binding affinities of TQ towards G-quadruplex DNA and ct-DNA were estimated using fluorescence titrations described in Section 2.4.3. Variable DNA concentrations were added to constant TQ and followed fluorometrically. Scatchard plots of r/C_f versus r were constructed. According to Scatchard, $r/C_f = nK - Kr$ where r is the number of moles of TQ bound to one mol of DNA (C_b/C_{DNA}), n is the number of equivalent binding sites per molecule and K is the binding affinity of TQ for those sites. The free and bound concentrations of TQ (C_f, C_b) were calculated using $C_f = C_{total}(1 - \alpha)$ and $C_b = C_{total} - C_f$, respectively, where C_{total} is the total TQ concentration at zero addition. The fraction of bound TQ (α) was calculated using the equation $\alpha = (F_f - F) / (F_f - F_b)$ where F_f, F and F_b are fluorescence intensities at zero addition, after each addition and at saturation, respectively. Scatchard plot gives a slope equals K and intercept equals nK.

2.4.5. Stoichiometry

Stoichiometry of TQ's interactions with G-quadruplex and ct-DNAs was determined using the molar ratio method. A 3.00 ml aliquot of TQ (5×10^{-5} M) or (5×10^{-4} M) was mixed with different amounts of G-quadruplex (1.44×10^{-4} M) or ct-DNA (1×10^{-7} M), respectively. Measurements were made in Tris–KCl buffer pH 7 4.

Solutions were scanned for their TQ fluorescence at emission λ_{max} of 330 nm and excitation λ_{max} of 295 nm. Plots of fluorescence versus molar ratios ([TQ] / [DNA]) were constructed.

2.4.6. Selectivity of TQ towards G-quadruplex

Selectivity of TQ towards G-quadruplex was investigated by mixing a 3.00 ml solution that is 10^{-7} M in Fl-G-quadruplex and 10^{-7} M TQ with 0.0, 10.0, 50.0 or 100.0 folds of hybridized telomere ds-DNA or ct-DNA in Tris–KCl-buffer pH 7.4. Resultant solutions were vortexed for 10 s, incubated at room temperature for 5 min and scanned for their fluorescence in the range of 500–700 nm using the emission and excitation wavelengths of Fl-G-quadruplex ($\lambda_{max} = 518$ and $\lambda_{max} = 494$ nm, respectively) and slit width of 5 nm.

2.4.7. Liquid and solid NMR

^{1}H NMR and ^{13}C NMR spectra of TQ (10^{-2} M) mixed with different amounts of G-quadruplex (10^{-2} M) were collected at 25 °C in deuterated ethylene glycol ($C_4H_4(OD)_2$) at observed frequencies of 399.731 and 100.512 MHz, respectively. ^{1}H NMR spectra were recorded using 45.0° pulse angle, 1.00 s relaxation delay, 2.049 s acquisition time and 6410.3 Hz spectral width into 64 repetitions. Decoupled ^{13}C NMR spectra were collected using 45.0° pulse angle, 1.0 s relaxation delay, 1.30 s acquisition time, 24,509 Hz spectral width and 0.5 Hz line broadening into 18,000 repetitions.

Solid ^{13}C NMR spectrum of ct-DNA was collected using 50.0 mg ct-DNA packed into the sample's rotor. TQ–ct-DNA complex was prepared by mixing 50.00 mg of DNA dissolved into 10.0 ml deionized water with 25.0 mg TQ dissolved in 0.5 ml ethanol. The solution was thoroughly mixed, incubated for 1 h then dried in vacuum. Resultant solid residue was packed into the sample's rotor and scanned for ^{13}C NMR. Spectra were collected at 25 °C using 5.00 s relaxation delay time, 0.04 s acquisition time, 6.00 μs pulse width, 40,322.6 Hz signal width into 8877 repetitions and line broadening of 40.00 Hz.

2.4.8. Melting temperature curves

Melting temperature curves for G-quadruplex, ct-DNA and their TQ adduct complexes were constructed using CD measurements. A 1.0 ml of telomeric G-quadruplex (2.76×10^{-6} M) or ct-DNA (35.00 μg/ml) in Tris–KCl-buffer, pH 7.4 was heated up from 25 to 95 °C in 5 °C increments applying 5.0 min incubation intervals. CD spectra were recorded in the range of 200–400 nm at each temperature.

TQ–G-quadruplex complex was prepared by mixing TQ (72.0 μl; 10^{-3} M) with G-quadruplex (48.0 μl; 5.74×10^{-4} M) while TQ–ct-DNA complex was prepared by mixing TQ (60.0 μl; 10^{-3} M) with ct-DNA (35.0 μl; 1000 μg/ml) and made up to 1.0 ml using Tris–KCl buffer pH 7.4. Solutions were scanned for their CD spectra and intensities at 292 nm for or at 278 and 273 nm were recorded. Melting temperature curves for TQ–G-quadruplex and TQ–ct-DNA were respectively constructed.

3. Results and discussion

3.1. UV–vis absorption spectrometry

Ethylene glycol has been reported as non-denaturizing and doesn't affect the conformation of DNA [58]. Therefore, it was used as a co-solvent to improve the solubility of TQ in our study. TQ was found stable in ethylene glycol over several days, if protected from light and kept in fridge. However, freshly prepared solutions were used throughout this study. The p-benzoquinones have four absorption bands in UV–vis region. A strong band at 250 nm (ε = 20,000) and a weak band at 300 nm (ε = 320) were ascribed to π–π* transitions. The other two bands are shown at 400–500 (ε = 20–30) and 540 nm (ε = 0.2) as very weak and attributed to n–π* singlet–singlet and singlet–triplet transitions, respectively [59]. In this work, we tested the effect of ethylene glycol on G-quadruplex confirmation using CD spectrometry. Ethylene glycol up to 20% was found ineffective as indicated in the provided supplementary materials. Therefore a 10% ethylene glycol was adopted in this study to improve the solubility of TQ.

Fig. 1a shows the UV–vis spectra of TQ in 10% ethylene glycol. The observed strong band at 258 nm and weak band at 295 nm are attributed to π–π* transitions. Bands at longer wavelengths are weak enough to not be observed. The effect of pH on TQ is also shown in Fig. 1a. TQ was shown to be stable in the pH range of 3–9. At pH >10, the 258 nm band dramatically decreased. The reason could be attributed to the conversion of TQ into the mono- and di-peroxy-p-thymoquinone resulted in the disappearance of the π bonds in the ring (C5 = C6, C2 = C3, Scheme 1) [60]. Since pH 7.4 is optimum for G-quadruplex formation and both ct-DNA and TQ are quite stable at this pH, it was used throughout this study.

Fig. 1b shows the UV–vis titration of TQ (10^{-3} M) with G-quadruplex DNA. The DNA band at 260 nm clearly interfered with the TQ absorption band at 258 nm. Therefore, the absorbance at 260 nm increased upon the additions of DNA. Applications of first and second derivative spectral processing to convolute the two bands did not succeed to resolve this interference. Subsequently, evidences on interactions between TQ and DNA were collected using circular dichroism, fluorescence, NMR, melting temperatures and docking simulations.

3.2. Circular dichroism

G-quadruplex forms several structural conformations depending on the sequence, length and environment of DNA. Human telomeric DNA

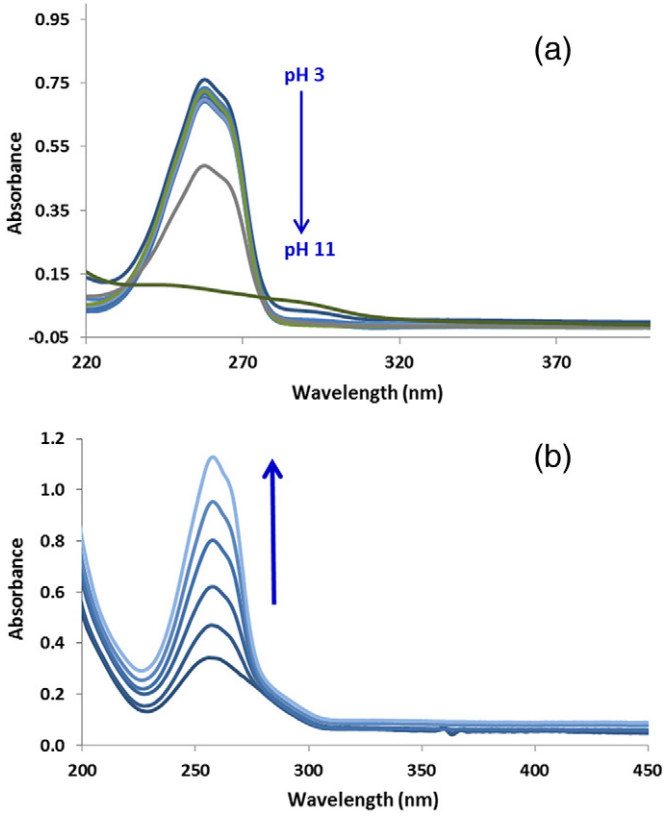

Fig. 1. (a) Effect of pH on TQ (1×10^{-5} M) using phosphate buffer (0.01 M), pH 3–11 and (b) titration of G-quadruplex (2×10^{-6} M) with TQ (10^{-3} M).

sequence forms antiparallel structures in the presence of Na^+ and hybrid structures in the presence of K^+ in solutions [61]. Fig. 2a shows the CD spectrum of our 22 base telomere G-quadruplex DNAs, $(AGGG(TTAGGG)_3)$. The appearance of a negative band centered at 235 nm and two positive bands at 253 and 293 nm indicated the formation of a hybrid (parallel–antiparallel) structure. Similar findings were reported by Ambrus and Tan [62,63].

Additions of TQ to this telomeric G-quadruplex structure resulted in the CD spectral changes shown in Fig. 2b. Intensities of the three bands at 235, 253 and 293 nm decreased upon additions of TQ at the beginning of titration. At higher concentrations of TQ, the positive band at 293 nm slightly red shifted and the positive band at 253 nm gradually transformed to a negative band at 258 nm.

Changes in intensity of CD spectra during titration have been correlated with the binding mode of drug's interaction on DNA. A decrease in CD intensity has been correlated with intercalation-binding mode while an increase was correlated with groove-binding mode [64]. Transformation of positive bands to negative ones has been correlated with conformational changes from hybrid to antiparallel G-quadruplex structure [8,65].

Subsequently, decreases in the CD intensities upon sequential additions of TQ in Fig. 2b may indicate an intercalation binding mode in which TQ binds to G-quartets by π–π stacking. Increase in CD intensity of the 293 nm band at higher TQ's concentration might indicate binding onto a different binding site (loop or G-quartet planes of G-quadruplex). The transformation of the 253 nm positive band to the negative one at 258 nm indicated a change in conformation of G-quadruplex from hybrid to antiparallel structure upon interaction with TQ [8,65].

These findings clearly indicated that TQ has interacted with G-quadruplex. The results suggest an intercalation binding of TQ on G-quadruplex through π–π stacking associated with structural change from hybrid into parallel conformation. They also suggest the presence of dependent binding sites on G-quadruplex.

3.3. Fluorescence spectrometry

Interaction of TQ with G-quadruplex DNA has been further confirmed using fluorescence spectrometry. Fluorescence spectra of TQ in Tris–KCl buffer are shown in Fig. 3a. TQ was found to give a weak fluorescence peak at 330 nm when excited at 295 nm. Excitation of TQ using its absorption band at 258 nm gave no fluorescence. The fluorescence peak at 330 nm is attributed π*–π transition and has been used for investigating the interaction of TQ with DNA [59].

Fig. 3a shows the changes in fluorescence spectra of TQ upon sequential additions of G-quadruplex. Gradual decrease in fluorescence intensity associated with slight red shift of the 330 nm band indicated

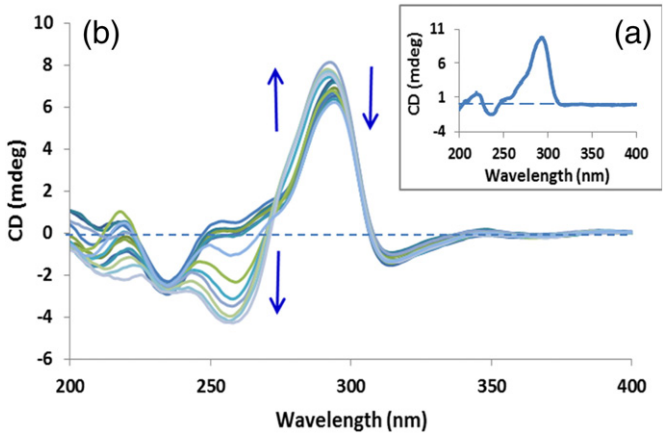

Fig. 2. (a) CD spectrum of telomeric G-quadruplex (3.6×10^{-6} M) and (b) CD titration of telomeric G-quadruplex (3.6×10^{-6} M) with TQ (1.0×10^{-3} M) in Tris–KCl buffer pH = 7.4.

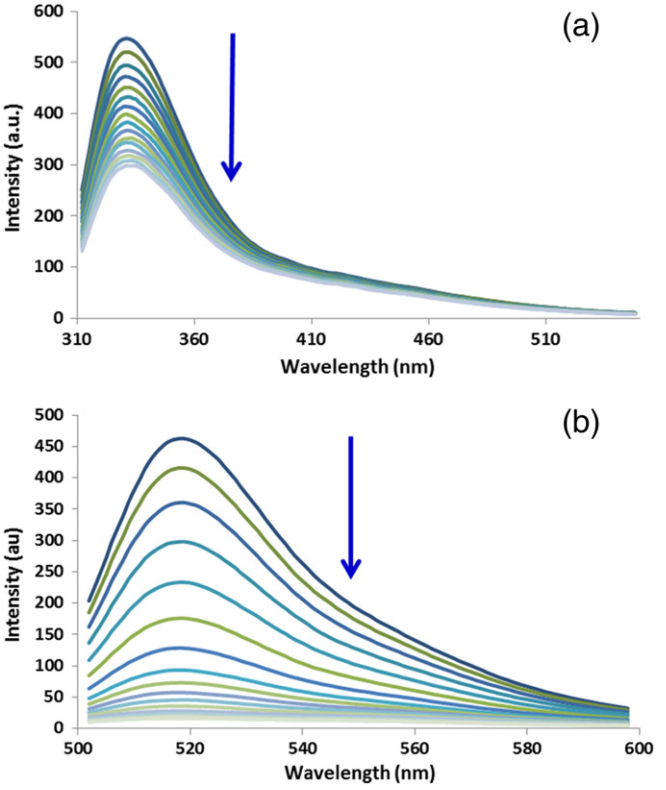

Fig. 3. Fluorescence titrations of (a) TQ (5×10^{-5} M) with telomeric G-quadruplex (1.44×10^{-4} M) and (b) Fl-G-quadruplex (1.98×10^{-6} M) with TQ ($1x10^{-3}$ M) in KCl-buffer pH = 7.4.

an interaction process between TQ and G-quadruplex DNA molecules. To exclude the effects of molecular aggregation and/or change in density of Molecular aggregation in Fl-G-quadruplex solution was also excluded by following up its fluorescence solution on fluorescence emission of TQ during titration, an experiment based on fluorescein labeled G-quadruplex was conducted.

Fl-G-quadruplex (5′-Fl-$AGGG(TTAGGG)_3$) has a fluorescence band at 518 nm when excited at 494 nm. Addition of TQ to FL-G-quadruplex resulted in quenching the fluorescence emission at 518 nm (Fig. 3b). This experiment indicated an interaction mechanism in which TQ bonded in close proximity to the fluorescein moiety of Fl-G-quadruplex molecule. Since FL molecule is connected to the 5′ prime, one may infer that TQ binds more adjacent to the TTA loop cavity rather than to the G-quartet interstitial planes. These results were confirmed by testing the effect of TQ on fluorescein compound. The supplementary data provided showed that TQ does not interact with fluorescein intensity at 518 nm over time. A 24 hours' time interval was found ineffective.

Therefore, results from fluorescence measurements confirmed an interaction process between TQ and G-quadruplex DNA. These results suggested that TQ has bonded in close proximity to the fluorescein moiety i.e. near to the TTA loop. The results are also consistent with findings obtained from CD measurements.

3.4. Binding affinity of TQ towards DNA

Binding affinities of TQ towards G-quadruplex and ct-DNA were estimated using Scatchard plots. A straight line Scatchard relationship of (r/C_f) versus r generally indicates the presence of one type of binding site or different types of independent and equivalent binding sites on DNA molecule. On the other hand, a nonlinear correlation curve indicates the presence of more than one type of dependent binding sites in which binding on one site suppresses/encourages binding on

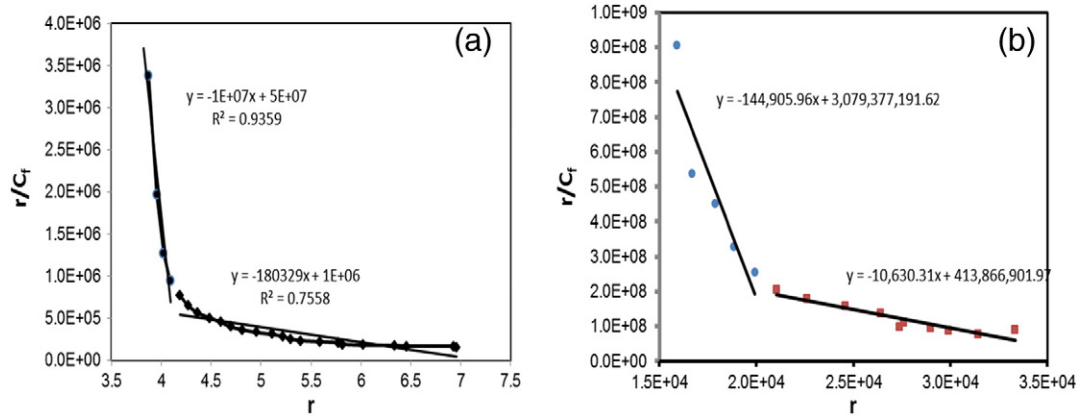

Fig. 4. Scatchard plots for the interactions of (a) TQ (5.0×10^{-5} M) with G-quadruplex (1.44×10^{-4} M) and (b) TQ (5×10^{-4} M) with ct-DNA (1×10^{-7} M). TQ fluorescence was recorded at 330 nm as λ_{max} of emission using 295 nm as λ_{max} of excitation.

the other site. This phenomenon is known as neighbor exclusion effect [66].

Fig. 4 shows Scatchard plots obtained from fluorescence titrations of TQ with G-quadruplex DNA (4a) and ct-DNA (4b). The two plots are nonlinear indicating the presence of more than one type of dependent binding sites. Nonlinear regressions of these plots were calculated using the Origin software. Interaction of TQ with G-quadruplex DNA revealed a binding constant $K = 6.88 \times 10^5\ M^{-1}$ and a number of binding sites n = 5.86 per each G-quadruplex molecule (Fig. 4a). Similarly interaction of TQ with ct-DNA revealed a binding constant $K = 3.82 \times 10^4\ M^{-1}$ and binding sites n = 31,065 per each ct-DNA molecule (Fig. 4b).

On the other hand, analyses of the nonlinear curves gave two intersecting lines indicating the presence of two types of binding sites on each DNA molecule. Linear regressions of the two lines on the TQ–G-quadruplex interaction curve revealed a high-affinity site, $K = 1.12 \times 10^7$ and a low-affinity site, $K = 1.80 \times 10^5\ M^{-1}$ with n = 6 and n = 5.5 binding sites per G-quadruplex molecule, respectively (Fig. 4a and Table 3). Similarly, linear regressions of the two lines on the TQ–ct-DNA interaction curve gave a high-affinity binding site, $K = 1.45 \times 10^5$ and a low affinity site, $K = 1.04 \times 10^4\ M^{-1}$ with $n = 2.13 \times 10^4$ and $n = 3.89 \times 10^4$ binding sites per ct-DNA molecule, respectively (Fig. 4b and Table 3) [67].

These results suggest that TQ intercalates to G-quadruplex and ct-DNA through π–π stacking on one or two types of dependent binding sites. Intercalation on the high affinity site seems to occur first, followed by the low affinity site. Both types of sites are having equivalent number of binding sites, $n \approx 6$ for G-quadruplex and $\approx 3 \times 10^4$ for ct-DNA. These values reflect one binding site per each two base pairs on G-quadruplex molecule and 1–2 binding sites per each base pair on ct-DNA molecule. The binding constants indicated that TQ has 20–80 higher affinity towards G-quadruplex compared to ct-DNA. The lower affinity of TQ towards ct-DNA may be attributed to the higher hydrophobicity of the ct-DNA's grooves compared to that between the G-quartets of G-quadruplex.

3.5. Stoichiometry of TQ interaction with G-quadruplex

Stoichiometric ratios of TQ:G-quadruplex and TQ:ct-DNA were estimated using the molar ratio method. Fig. 5 shows the variations of fluorescence intensities of TQ at 330 nm versus molar ratio [DNA] / [TQ]. Two stoichiometric ratios were identified for the interaction of TQ with each of G-quadruplex and ct-DNA.

G-quadruplex formed two stoichiometric ratios around 1:6 and 1:12 indicating the presence of two types of binding sites with n = 6–7 sites per G-quadruplex molecule (Fig. 5a). The two ratios for ct-DNA indicated two types of binding sites with $n = 2.410^4$ and 4.4×10^4 (Fig. 5b). These values are roughly equivalent to one binding site per each two base pairs on G-quadruplex molecule and 1–2 binding sites per each base

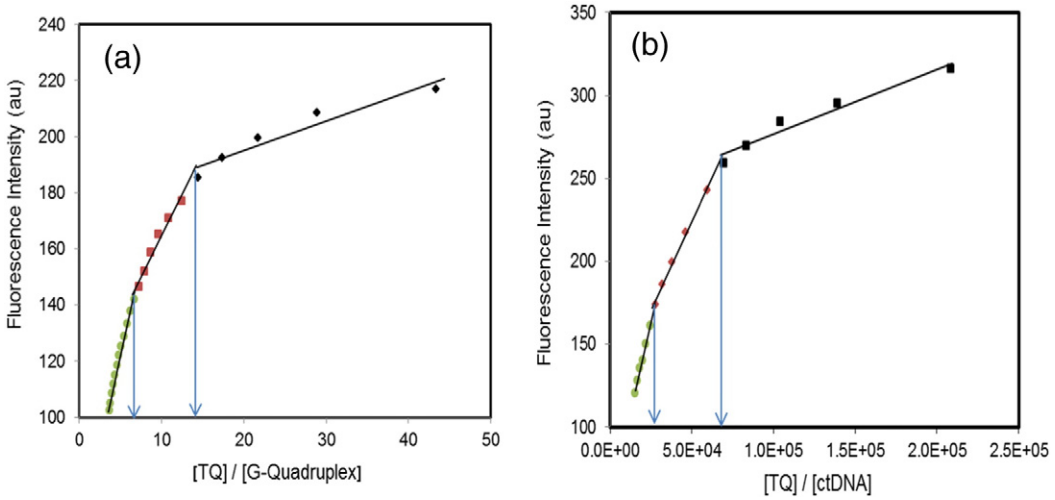

Fig. 5. Molar ratio methods for the interactions of: (a) TQ (5.0×10^{-5} M) with G-quadruplex (1.44×10^{-4} M) and (b) TQ (5×10^{-4} M) with ct-DNA (1×10^{-7} M). TQ fluorescence was recorded at 330 nm as λ_{max} of emission using 295 nm as λ_{max} of excitation.

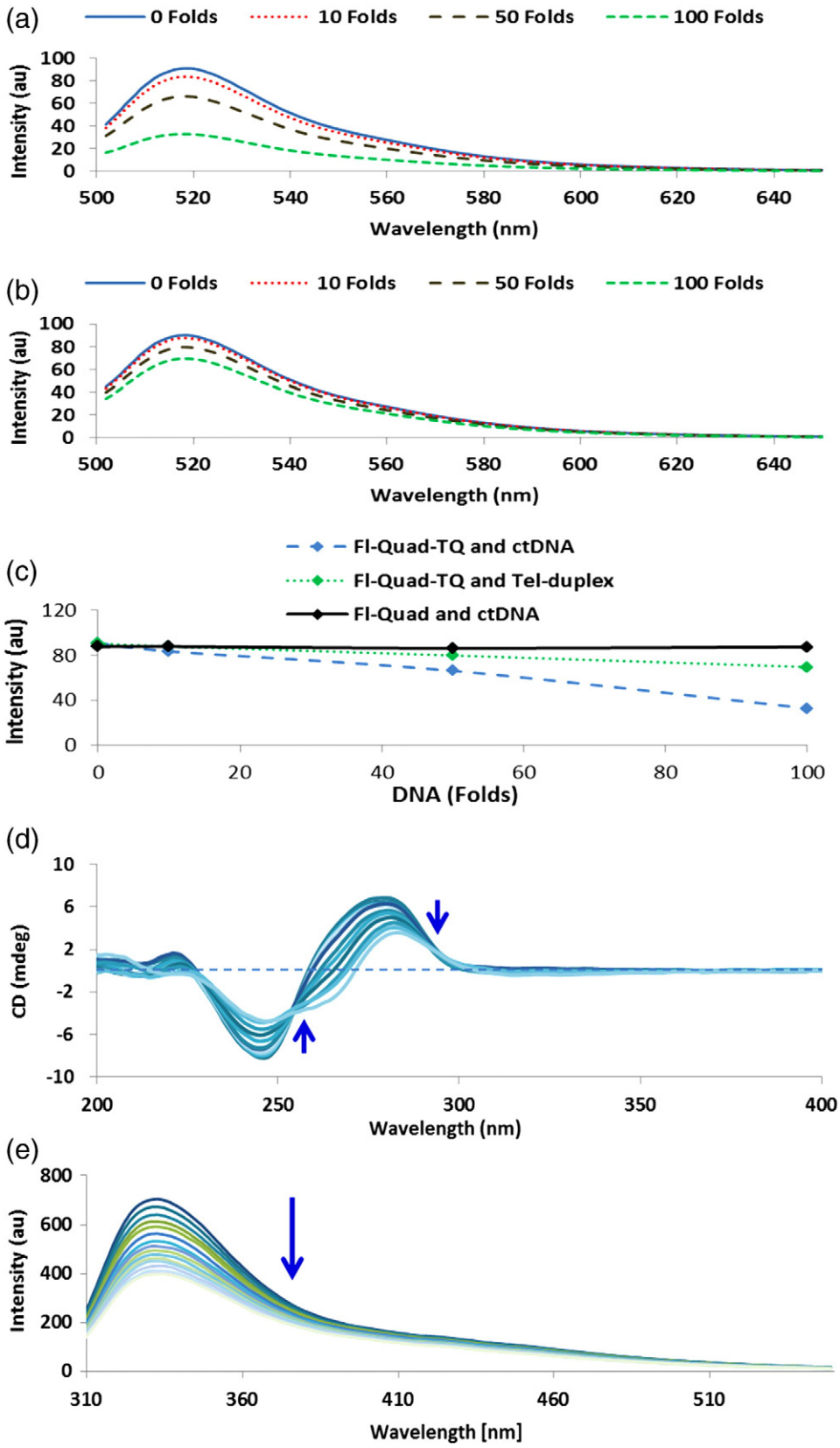

Fig. 6. Effect of adding 0, 10, 50 and 100 concentration folds of ct-DNA and telomere duplex as interfering species on TQ–Fl-G-quadruplex complex. (a) Effect of adding ct-DNA to a solution prepared by mixing equal volumes (100 μl) of TQ and Fl-G-quadruplex (5×10^{-10} M each). (b) Effect of adding telomere duplex to a solution prepared by mixing equal volumes (100 μl) of TQ and Fl-G-quadruplex (5×10^{-10} M each). The total volume was made up to 2.00 ml using Tris–KCl buffer pH 7.4. (c) Changes in fluorescence intensity of Fl-G-quadruplex (5×10^{-7} M) upon additions of telomere duplex and ct-DNA in the presence and absence of TQ, (d) CD titration of ct-DNA (4×10^{-9} M; 50 μg/ml) with TQ (5×10^{-5} M), (e) fluorescence titration of TQ (5×10^{-5} M) with ct-DNA (8×10^{-8} M; 1000 μg/ml). All measurements were made in Tris–KCl buffer pH = 7.4.

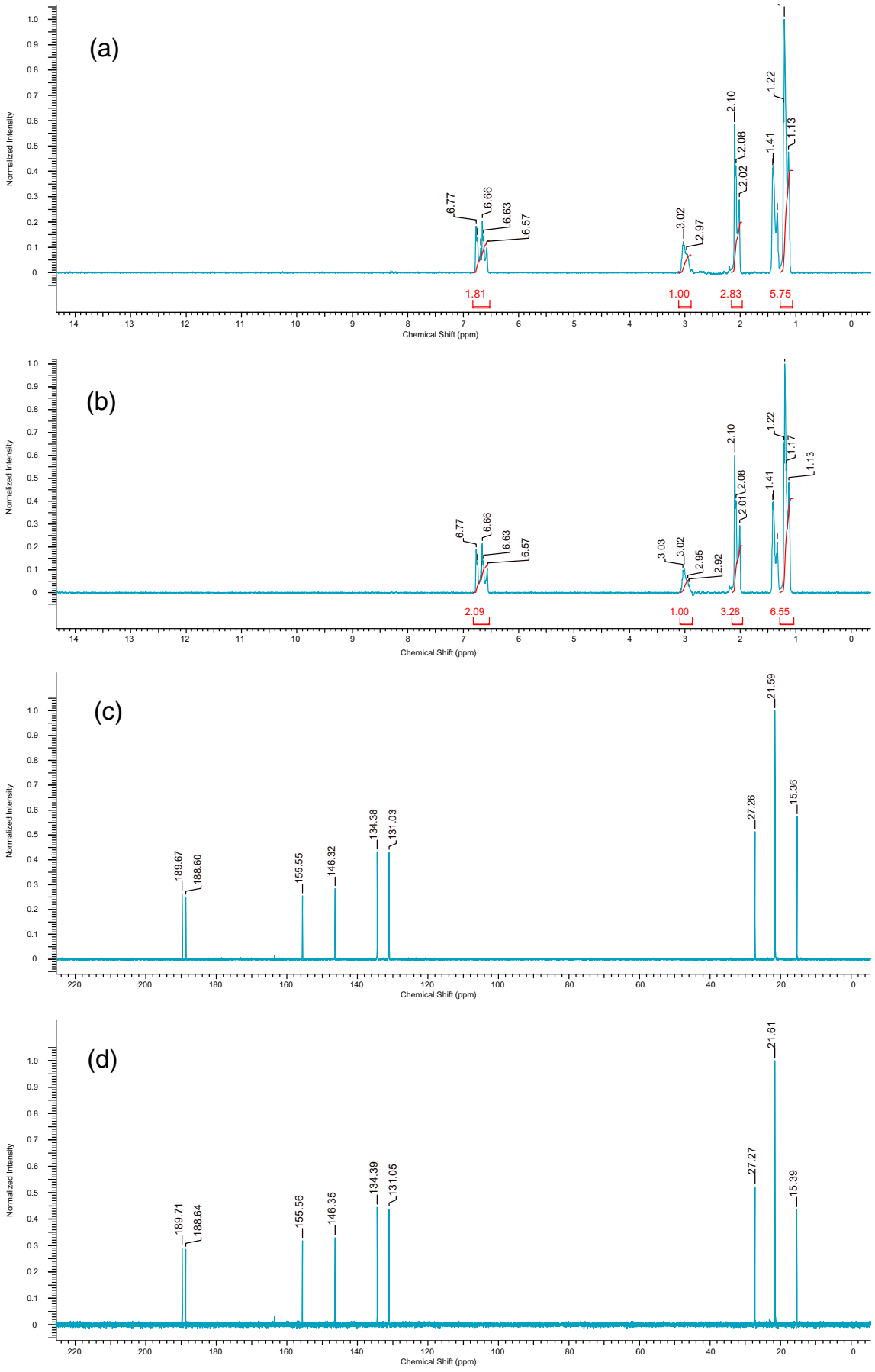

Fig. 7. (a) ^{1}H NMR spectrum of TQ (1×10^{-2} M), (b) ^{1}H NMR spectrum of 1:1 TQ: G-quadruplex, (c), ^{13}C NMR spectrum of TQ (1×10^{-2} M) and (d) ^{13}C NMR spectrum of 1:1 TQ–G-quadruplex. Spectra are measured in ethylene glycol $(CH_2OD)_2$.

Table 1
Assignments of ^{1}H and ^{13}C NMR signals of TQ and changes in their chemical shift upon complex formation with G-quadruplex.

^{1}H NMR			^{13}C NMR		
$^{\delta}$ppm	Assignment	$^{\Delta\delta}$ppm	$^{\delta}$ppm	Assignment	$^{\Delta\delta}$ppm
1.13	Methyl protons of the isopropyl group	0.01	21.59	C_8, isopropyl group	0.02
3.02	Methylene proton of the isopropyl group	0.01	27.26	C_7, isopropyl group	0.01
2.97		0.02			
2.08	Methyl protons of the methyl group	0.0	15.36	C_9, methyl group	0.03
6.57	Methylene protons of the benzoquinone ring	0.0	131.03	C_6, benzoquinone ring	0.02
6.63		0.0	134.38	C_5, benzoquinone ring	0.01
6.66		0.0	146.32	C_4, benzoquinone ring	0.03
6.77		0.0	155.55	C_3, benzoquinone ring	0.01
			188.60	C_2, carbonyl carbon	0.04
			189.67	C_1, carbonyl carbon	0.04

pair on ct-DNA. These results are consistent with the number of binding sites calculated using Scatchard plots [68].

The small size, planarity of π system and flexibility of the isopropyl group may explain why six TQ molecules are bound to each site on G-quadruplex molecule. TQ is possibly intercalated to G-quadruplex by π–π stacking. It seems from our results that the high affinity site is first occupied by six TQ molecules followed by another six on the low affinity site in a dependent fashion. A similar scenario could be used to interpret binding of TQ on ct-DNA binding sites.

3.6. Selectivity of TQ towards G-quadruplex

Selectivity of TQ towards G-quadruplex was estimated using 0.0, 10.0, 50.0 or 100.0 folds of hybridized telomere ds-DNA or ct-DNA, added to the complex formed by mixing equimolar amounts of TQ and Fl-G-quadruplex (Section 2.4.6). Fluorescence intensity at 518 nm was found to slightly decrease with the increasing concentrations of telomere duplex or ct-DNA interfering species from zero to 100 folds (Fig. 6a and b). If duplex DNAs are interfering, they would have increased the fluorescence intensity by taking out TQ from the complex and releasing Fl-G-quadruplex free. In another experiment, we tested the effect of telomere duplex and ct-DNA on Fl-G-quadruplex in the absence of TQ. No change in fluorescence intensity was observed indicating no interaction between duplex DNA and Fl-G-quadruplex (Fig. 6c, also see the Supplementary material). In a third experiment, interaction of TQ with ct-DNA was confirmed using CD and fluorescence titrations. Changes in CD spectra and decrease in fluorescence intensity at 330 nm indicated that ct-DNA interacts with TQ (Fig. 6d and e).

These results are surprising. It indicates that TQ selectively binds to G-quadruplex. Decrease in fluorescence intensity of TQ–Fl-G-quadruplex mixture upon addition of duplex DNA may also indicate that addition of duplex DNA enhanced the interaction of TQ with Fl-G-quadruplex. The reason may be attributed to the increase of solution crowdedness that pushes TQ towards G-quadruplex. Other yet unknown reasons may also possible.

Selectivity coefficients were calculated according to Wang et al. by measuring the fluorescence signals in the presence and absence of interfering molecules [69]. Selectivity coefficients of 2.80×10^{-3} and 3.33×10^{-3} were obtained for telomere duplex and ct-DNA, respectively. These results suggest that TQ selectively binds and stabilizes G-quadruplex DNA over duplex DNA.

3.7. NMR spectrometry

Interaction of TQ with G-quadruplex and ct-DNA was further confirmed using ^{1}H NMR and ^{13}C NMR. Spectra were collected in ethylene glycol – as a safe media for DNA conformation – using the experimental parameters described in Section 2.4.7 [58]. A second experiment was performed in aqueous solution using a 700 MHz NMR spectrometer. The results of this experiment are provided as Supplementary material and planned for a future paper. In additions, a solid state NMR experiment was performed to further confirm interaction of TQ with ct-DNA.

3.7.1. Liquid NMR spectra

Fig. 7 shows the ^{1}H NMR spectrum of TQ collected in ethylene glycol. The quartet and multiplet signals at 1.13 ppm and 3.02 ppm are attributed to the methyl and methylene protons of the isopropyl group, respectively. The signal at 2.08 pm is attributed to the methyl protons of the methyl group. The two doublets at 6.52 and 6.66 ppm are attributed to the two methylene protons on the benzoquinone ring. Splitting of these signals is possibly attributed to partial coupling with the adjacent methyl protons. Signals' integration supported our assignment. The ethylene glycol protons were shown at 3.716 ppm and removed from the pattern for clarification.

Fig. 7c shows the ^{13}C NMR of TQ. The signals at 21.59 and 27.26 ppm are attributed to the methyl carbon of the isopropyl group (C_8) and the methylene carbon of the isopropyl group (C_7), respectively. The signal at 15.36 pm is attributed to the methyl carbon of the methyl group (C_9) while the signals at 131.03, 134.38, 146.32 and 155.55 ppm are attributed to carbons C_3, C_6, C_5 and C_2 of the benzoquinone ring. The signals at 188.60 and 189.67 ppm are attributed to the carbonyl carbons (C_4 and C_1). The methylene carbon of ethylene glycol was shown at 63.71 ppm and removed for clarification.

Addition of G-quadruplex to TQ resulted in up-field shifting the ^{1}H NMR signals at 3.02 and 2.97 ppm by $\pm(0.01–0.02)$ ppm and the ^{13}C NMR signals by 0.01–0.04 ppm (Fig. 7c and d and Table 1). These findings are similar to the findings reported by Boudreau et al. [70]. Up-field shifts of protons and carbons NMR signals of TQ can be attributed to their shielding upon intercalation with G-quadruplex. Structural effects such as steric compression, base stacking or ring current are normally responsible for shielding effects. The magnitude of shielding and subsequently changes in chemical shifts are also dependent on the concentration of DNA added to TQ [70].

In the second experiment, changes in ^{1}H NMR signals of DNA upon binding with TQ were investigated in aqueous buffer solution. ^{1}H NMR spectrum of 5.0 μmol G-quadruplex is shown in the Supplementary Fig. 2. The signals in the ranges of 5.00–8.00 and 8.00–10.00 ppm are attributed to the aromatic protons of nucleotide bases and amino protons. The signals in the range of 10.00–12.00 ppm are attributed to the imino protons from Hoogsteen hydrogen bonding between guanines in the tetrads in G-quadruplex. Addition of 0.75 μmol TQ to the G-quadruplex resulted in significant decreases in intensities of amino and imino protons associated with up-field shifts by around 0.1 ppm.

Changes in chemical shifts of the above signals and decreases in their intensities indicated structural alteration of G-quadruplex upon binding with TQ. Decreases in signals' intensities of imino proton have been rationalized based on loss of hydrogen bonding and disrupting structural

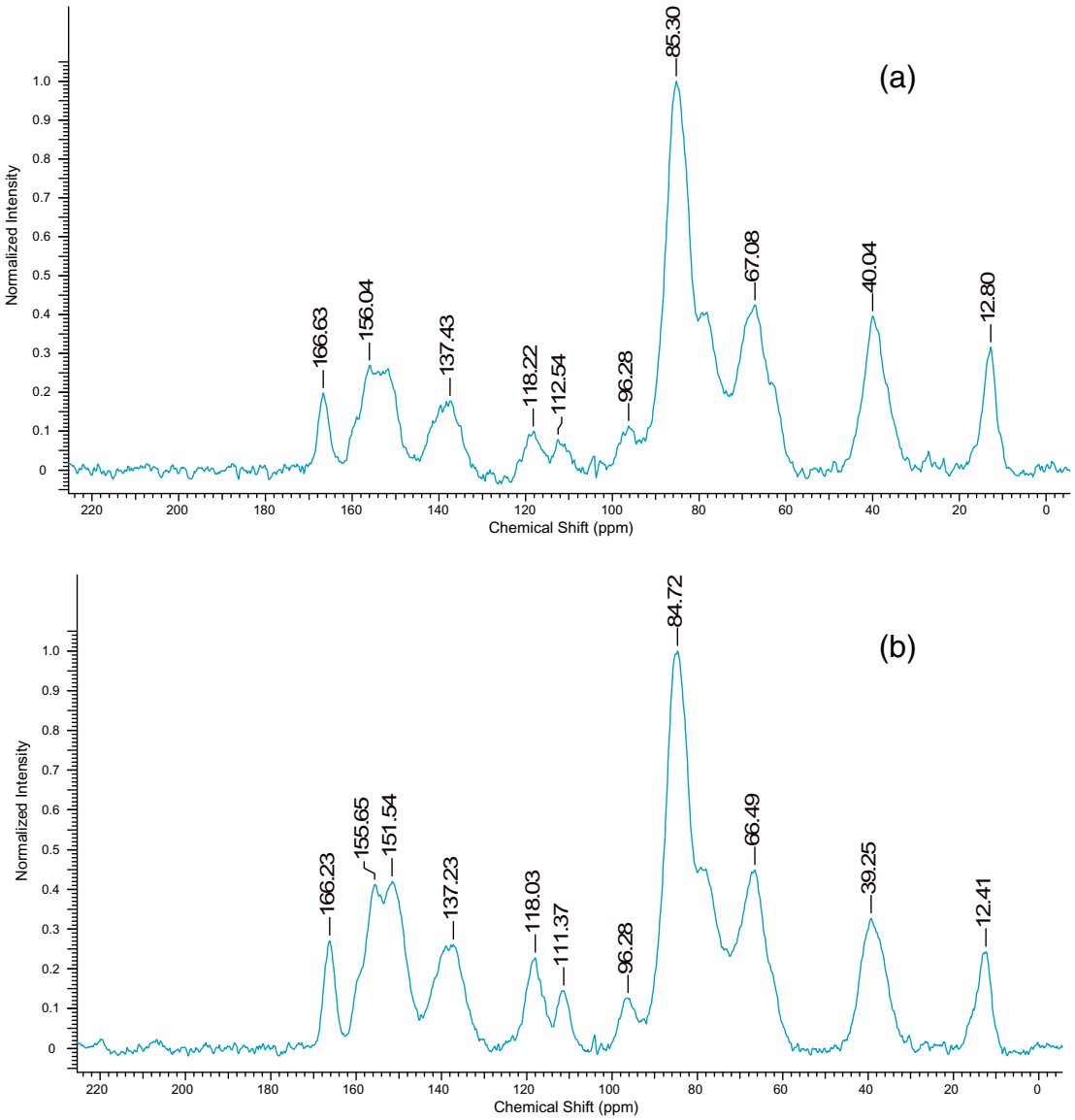

Fig. 8. Solid state ^{13}C NMR spectra of (a) ct-DNA (50.00 mg) and (b) TQ–ct-DNA complex (50.00 mg ct-DNA mixed with 25.00 mg TQ).

integrity of G-tetrads. These effects result in weakening the hydrogen bonding upon addition of TQ. These findings are consistent with the above results from CD and NMR and indicate that TQ is possibly intercalated to G-quartets through π–π stacking. Similar findings were reported by Walter and coworkers [71].

3.7.2. Solid NMR spectra

Solid NMR is a well suited tool for characterizing DNA interactions with small molecules. In this experiment, interaction of TQ with ct-DNA was further confirmed using solid-state NMR. Fig. 8a shows the ^{13}C solid NMR spectra of ct-DNA and TQ-ct-DNA complex collected according to the experimental parameters described in Section 2.4.7. Aliphatic carbons of sugar are located in the up field side of the spectra whereas quaternary carbons of nucleotide basses are on the downfield side. Signals around 50, 30, 35, and 60 ppm are attributed to the hemiacetal C1′, aliphatic methylene C2′, secondary phosphate ester C3′, secondary hemiacetal ether C4′ and the primary phosphate ester C5′, respectively (Table 2) [72].

Fig. 8b and Table 2 also show changes in chemical shifts upon complexation with TQ. Carbons were de-shielded by magnitudes ranged in 0.20–1.17 ppm. The C2′ carbon class exhibited the largest changes in chemical shifts (−0.79 ppm) compared to C1′, C3′, C4′ and C5′ (−0.58–0.59 ppm). These changes were attributed to alterations in sugar pucker, glycosyl torsion angles and dynamic pseudorotational states occupied by DNA sugars [72]. Carbons of nucleotide bases were also shifted downfield by larger Δδ values for thymine and adenine bases (−1.17 and − 0.39 ppm, respectively) compared to G and C (−0.39–0.4 ppm) (Table 2). These changes in solid NMR spectra indicated a binding interaction of TQ to ct-DNA. Larger changes in chemical shifts of A–T signals may indicate a preferentially binding of TQ to A–T bases. Changes in sugar resonances are consistent with changes in nucleotide bases.

These findings support our above conclusions about structural changes in DNA upon complexation with TQ. Changes in chemical shifts are similar to previously reported magnitudes of chemical shift's changes [71,73]. Results also suggest that TQ is preferentially intercalated on A–T minor groove of the oligonucleotides.

3.8. Melting temperature (T_m)

Melting temperature, the temperature at which hybridized DNA is denaturized, is used to evaluate capabilities of small molecules to

Table 2
Assignment of solid ^{13}C NMR signals of ct-DNA and change in their chemical shift upon complex formation with TQ. Chemical shifts in parenthesis are values reported in literature.

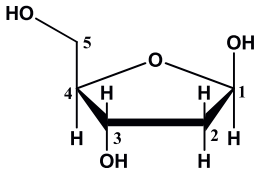

$^{\delta}$ppm	Assignment	$\Delta\delta_{ppm}$
12.80	Thymine-CH_3	−0.39
40.04	Aliphatic methylene C2′	−0.79
67.08	Hemiacetal Cl′	−0.59
85.30	Secondary phosphate ester C3′ and secondary hemiacetal ether C4′	−0.58
96.28	Primary phosphate ester C5′ or cytosine C5 (94.4)	–
112.54	Thymine C5 (112.9)	−1.17
118.22	Adenine C5 (117.3)	−0.19
137.43	Adenine C8 (137.3) or thymine C6 (136.3)	−0.20
151.93	Adenine C2 & C4 (149.4)	−0.39
156.04	Adenine C6 (156.1) Less possible: Guanine C2 & C4 (157.1) or thymine C2 (154.4)	−0.39
166.63	Cytosine C4 (168.7)	−0.40

stabilize DNA. The capability of TQ to stabilize G-quadruplexes and ct-DNA was estimated using CD measurements and 1:1 (TQ:DNA) molar ratios (see Section 2.4.2). Bigger T_m values could have been obtained if bigger molar ratio was used. Fig. 9 shows the melting temperature curves of G-quadruplex, ct-DNA and their TQ complexes. The figure shows that TQ stabilized G-quadruplex by $\Delta T_m = +5.6$ °C, ($T_{m,TQ-G\text{-}quadruplex} - T_{m,G\text{-}quadruplex} = 71.2 - 65.6 = +5.6$ °C) and destabilized ct-DNA by $\Delta T_m = -5.1$ °C, ($T_{m,TQ-ct\text{-}DNA} - T_{m,ct\text{-}DNA} = 80.0–85.1 = -5.1$ °C). These results indicated that TQ stabilized G-quadruplex and destabilized ct-DNA structures by nearly the same magnitudes. Similar ΔT_m values were obtained by Ma and coworkers [74]. Stabilizing G-quadruplex and destabilizing ct-DNA are consistent with the values of binding constants obtained from Scatchard plots (Table 3). TQ showed 100 times higher binding affinity towards G-quadruplex over duplex. Destabilization of duplex DNA by TQ ($K \cong 10^4$) is similar to results reported for adriamycin and macrocyclic lanthanide complexes as DNA destabilizers while their binding constants $K \cong 10^7$ and ~10^5 M^{-1}, respectively [75–77].

Thus, our melting temperature experiment gave an additional evidence for the preferential selectivity of TQ to stabilize G-quadruplex over duplex DNA. It also supported the suggestion of binding to G-quartet of G-quadruplex in the vicinity of the TTA loops by π–π stacking.

3.9. Molecular docking simulation

To further assure the above results, we found it important to get an additional proof on stabilizing G-quadruplex by TQ using molecular docking simulation. DOCK 6.4 program was used for docking simulation [78] and discovery studio program [79] was used for constructing the TQ molecule. G-quadruplex structure was taken from the human telomeric intramolecular quadruplex structure (PDB ID # 3UYH). The 3D grid box covered the whole DNA with size of $3.5 \times 4.5 \times 3.9$ nm^3. Scores for docking simulation are the approximate binding energies. Docking score for the ligand on DNA was represented by various energy terms such as electrostatic energy, van der Waals energy, and solvation energy.

Fig. 10 shows that TQ binds to G-quadruplex on two binding sites located near the loop regions. The first binding site is close to T17, T18 and A19 loop with grid score of −19.5 kcal/mol (low affinity site). The second binding site is in the T11, T12 and A13 loop with grid score of −26.2 kcal/mol (high affinity site).

These findings are in good agreement with our results obtained by NMR, fluorescence and CD measurements. These results are also in good agreement with the results obtained by Di Leva et al. [80].

4. Conclusion

TQ has been documented in numerous cancer studies in animal models, culture and xenografted tumors to possess chemo-preventive and chemotherapeutic antitumor effects. Underlying mechanisms based on inductions of cell cycle arrest, apoptosis, oxidative damage of cellular macromolecules, blockade of tumor angiogenesis and suppressions in migration, invasion and metastasis of cancer cells were proposed. Various molecular targets were provided in support of each mechanism. Direct oxidative damage of DNA was not supported by the low redox potential of TQ compared to the redox potentials of guanine and adenine bases on DNA.

In this work, human telomere G-quadruplex DNA was investigated as a molecular target for TQ using UV–vis, CD, fluorescence, NMR, melting temperature and molecular docking simulation. Spectral changes, melting temperature curves and docking simulations provided evidences for the interaction of TQ with G-quadruplex.

Fluorescence and NMR results indicated that TQ bound close to the TTA loop of G-quadruplex. Scatchard plots revealed nonlinear regression with binding constant $K = 6.88 \times 10^5$ M^{-1} and n = 5.86 binding sites per G-quadruplex molecule. Analysis of Scatchard plot

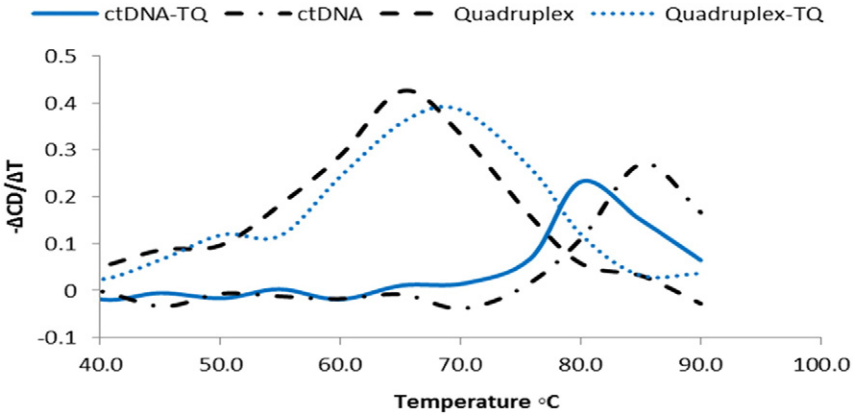

Fig. 9. Melting temperature curves of G-quadruplex (– – –), TQ–G-quadruplex complexes (••••••••••), ct-DNA (——) and TQ–ct-DNA complex (—·—·—).

Table 3
Binding constants and number of binding sites per G-quadruplex molecule and ct-DNA molecule towards TQ.

Binding site	G-quadruplex[a]			ct-DNA[a]		
	Binding constant K (M^{-1})	Number of binding sites per DNA molecule (n)		Binding constant K (M^{-1})	Number of binding sites per DNA molecule (n)	
		S.M.	M.R.M.		S.M.	M.R.M.
Site 1	1.8×10^5	5.5	7.2	1.06×10^4	2.13×10^4	2.43×10^4
Site 2	1.12×10^7	6.0	6.7	1.45×10^5	3.89×10^4	4.44×10^4

S.M. refers to Scatchard method and M.R.M. refers to molar ratio method.
[a] Calculations are based on molecular weights of 6967 and 10^7 Da for G-quadruples and ct-DNA, respectively.

into two lines revealed two binding sites with $K = 1.12 \times 10^7$ and 1.80×10^5 M^{-1} and n = 6 and 5.5 per G-quadruplex molecule, respectively. Similarly interaction of TQ with ct-DNA revealed nonlinear Scatchard's plot with $K = 3.82 \times 10^4$ M^{-1} and n = 31,065. Analysis of this plot into two linear regressions gave $K = 1.04 \times 10^4$ and 1.45×10^5 M^{-1} with $n = 2.4–4.4 \times 10^4$. These numbers are roughly equivalent to two sites per each G-quartet on G-quadruplex and 1–2 binding sites per each base pair on ct-DNA. Spectral changes gave no evidence for oxidation of G-quadruplex nucleotide bases by TQ.

Melting temperature curves indicated that TQ stabilized human telomere G-quadruplex by +5.6 °C while destabilized duplex ct-DNA by −5.1 °C. Selectivity coefficients of 2.8×10^{-3} and 3.33×10^{-3} were respectively obtained for TQ's interaction with telomere G-quadruplex over duplex human telomere DNA and ct-DNA.

Docking simulation confirmed the presence of two types of binding sites on G-quadruplex close to T17–T18–A19 and T11–T12–A13 loops. The first site is of low affinity with grid scores of −19.5 kcal/mol while the second one is of high affinity with grid score of and −26.2 kcal/mol.

These results indicated that TQ can possibly act as G-quadruplex stabilizer and subsequently contribute to telomerase inhibition, cell apoptosis and inhibition of cancer proliferation. The results represent a change in reported anticancer mechanisms of TQ and in the paradigm of structural features for G-quadruplex stabilizers previously reported.

Acknowledgement

The authors are gratefully acknowledging the financial support of the Emirates Foundation under grant # 2010/122 allocated to the principal author. Without their support, this work would have not been executed.

Appendix A. Supplementary data

Supplementary data to this article can be found online at http://dx.doi.org/10.1016/j.bbagen.2014.10.018.

References

[1] C.C. Woo, L.P. Kumar, G. Sethi, K.H.B. Tan, Thymoquinone: potential cure for inflammatory disorders and cancer, Biochem. Pharmacol. 83 (2012) 443–451.
[2] S. Banerjee, S. Padhye, A. Azmi, Z. Wang, P.A. Philip, O. Kucuk, F. Sarkar, R. Mohammad, Review on molecular and therapeutic potential of thymoquinone in cancer, Nutr. Cancer 62 (2010) 938–946.
[3] H.A. Johnson, L.L. Rogers, M.L. Alkire, T.G. McCloud, J.L. McLaughlin, Bioactive monoterpenes from *Monarda fistulosa* (Lamiaceae), Nat. Prod. Lett. 11 (1998) 241–250.
[4] D.R. Worthen, O.A. Ghosheh, P.A. Crooks, The in vitro anti-tumor activity of some crude and purified components of black seed, *Nigella sativa* L, Anticancer Res. 18 (1998) 1527–1532.
[5] J. Kundu, K.S. Chun, O.I. Aruoma, J.K. Kundu, Mechanistic perspectives on cancer chemopreventive/chemotherapeutic effects of thymoquinone, Mutat. Res. Fundam. Mol. Mech. Mutagen. 768 (2014) 22–34.
[6] H.U. Gali-Muhtasib, W.G. Abou Kheir, L.A. Kheir, N. Darwiche, P.A. Crooks, Molecular pathway for thymoquinone-induced cell-cycle arrest and apoptosis in neoplastic keratinocytes, Anticancer Drugs 15 (2004) 389–399.
[7] V. Cecarini, L. Quassinti, A. Di Blasio, L. Bonfili, M. Bramucci, G. Lupidi, M. Cuccioloni, M. Mozzicafreddo, M. Angeletti, A.M. Eleuteri, Effects of thymoquinone on isolated and cellular proteasomes, FEBS J. 277 (2010) 2128–2141.
[8] N.K. Effenberger, R. Schobert, Combinatorial effects of thymoquinone on the anticancer activity of doxorubicin, Cancer Chemother. Pharmacol. 67 (2011) 867–874.
[9] C.C. Woo, S.Y. Loo, G. Veronica, C.W. Yap, G. Sethi, A.P. Kumar, K.H. Tan, Anticancer activity of thymoquinone in breast cancer cells: possible involvement of PPARg pathway, Biochem. Pharmacol. 82 (2011) 464–475.
[10] M. Alhosin, A. Abusnina, M. Achour, T. Sharif, C. Muller, J. Peluso, T. Chataigneau, C. Lugnier, V.B. Schini-Kerth, C. Bronner, G. Fuhrmann, Induction of apoptosis by thymoquinone in lymphoblastic leukemia Jurkat cells is mediated by a p73-dependent pathway which targets the epigenetic integrator UHRF1, Biochem. Pharmacol. 79 (2010) 1251–1260.
[11] S.H. Jafri, J. Glass, R. Shi, S. Zhang, M. Prince, H.H. Kleiner, Thymoquinone and cisplatin as a therapeutic combination in lung cancer: in vitro and in vivo, J. Exp. Clin. Cancer Res. 29 (2010) 87.
[12] S. Rooney, M.F. Ryan, Effects of alpha-hederin and thymoquinone, constituents of *Nigella sativa*, on human cancer cell lines, Anticancer Res. 25 (2010) 2199–2204.

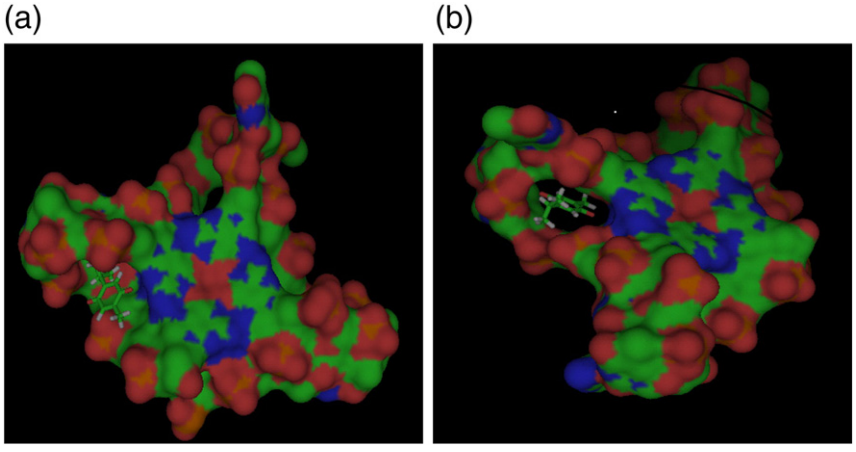

Fig. 10. Docking of TQ molecule on G-quadruplex structure. TQ is intercalated on two binding sites close to (a) T17, T18 and A19 loop with grid score of −19.5 kcal/mol (low affinity site) and (b) T11, T12 and A13 loop with grid score of −26.2 kcal/mol (high affinity site).

[13] N. El-Najjar, M. Chatila, H. Moukadem, H. Vuorela, M. Ocker, M. Gandesiri, R. Schneider-Stock, H. Gali-Muhtasib, Reactive oxygen species mediate thymoquinone-induced apoptosis and activate ERK and JNK signaling, Apoptosis 15 (2010) 183–195.
[14] M. Roepke, A. Diestel, K. Bajbouj, D. Walluscheck, P. Schonfeld, A. Roessner, R. Schneider-Stock, H. Gali-Muhtasib, Lack of p53 augments thymoquinone-induced apoptosis and caspase activation in human osteosarcoma cells, Cancer Biol. Ther. 6 (2007) 160–169.
[15] P.S. Koka, D. Mondal, M. Schultz, A.B. Abdel-Mageed, K.C. Agrawal, Studies on molecular mechanisms of growth inhibitory effects of thymoquinone against prostate cancer cells: role of reactive oxygen species, Exp. Biol. Med. 235 (2010) 751–760.
[16] D. Xu, Y. Ma, B. Zhao, S. Li, Y. Zhang, S. Pan, Y. Wu, J. Wang, D. Wang, H. Pan, L. Liu, H. Jiang, Thymoquinone induce G2/M arrest, inactivate PI3K/Akt and nuclear factor–kB pathways in human cholangiocarcinomas both in-vitro and in-vivo, Oncol. Rep. 32 (2014) 2063–2070.
[17] M. Motaghed, F.M. Hassan, S.S. Hamid, Thymoquinone regulates gene expression levels in the estrogen metabolic and interferon pathways in MCF7 breast cancer cells, Int. J. Mol. Med. 33 (2014) 8–16.
[18] H. Gali-Muhtasib, M. Diab-Assaf, C. Boltze, J. Al-Hmaira, R. Hartig, A. Roessner, R. Schneider-Stock, Thymoquinone extracted from black seed triggers apoptotic cell death in human colorectal cancer cells via a p53-dependent mechanism, Int. J. Oncol. 25 (2004) 857–866.
[19] S.A. Arafa, Q. Zhu, Z.I. Shah, G. Wani, B.M. Barakat, I. Racoma, M.A. El-Mahdy, A.A. Wani, Thymoquinone up-regulates PTEN expression and induces apoptosis in doxorubicin resistant human breast cancer cells, Mutat. Res. 706 (2011) 28–35.
[20] H. Gali-Muhtasib, D. Kuester, C. Mawrin, K. Bajbouj, A. Diestel, M. Ocker, C. Habold, C. Foltzer-Jourdainne, P. Schoenfeld, B. Peters, M. Diab-Assaf, U. Pommrich, W. Itani, H. Lippert, A. Roessner, R. Schneider-Stock, Thymoquinone triggers inactivation of the stress response pathway sensor CHEK1 and contributes to apoptosis in colorectal cancer cells, Cancer Res. 68 (2008) 5609–5618.
[21] J. Kundu, B.Y. Choi, C.H. Jeong, J.K. Kundu, K.S. Chun, Thymoquinone induces apoptosis in human colon cancer HCT116 cells through inactivation of STAT3 by blocking JAK2- and Src-mediated phosphorylation of EGF receptor tyrosine kinase, Oncol. Rep. 32 (2014) 821–828.
[22] M.A. El-Mahdy, Q. Zhu, Q.E. Wang, G. Wani, A.A. Wani, Thymoquinone induces apoptosis through activation of caspase-8 and mitochondrial events in p53-null myeloblastic leukemia HL-60 cells, Int. J. Cancer 117 (2005) 409–417.
[23] F. Li, P. Rajendran, G. Sethi, Thymoquinone inhibits proliferation, induces apoptosis and chemosensitizes human multiple myeloma cells through suppression of signal transducer and activator of transcription 3 activation pathway, Br. J. Pharmacol. 161 (2010) 541–554.
[24] G. Sethi, K.S. Ahn, B.B. Aggarwal, Targeting nuclear factor-kappa B activation pathway by thymoquinone: role in suppression of antiapoptotic gene products and enhancement of apoptosis, Mol. Cancer Res. 6 (2008) 1059–1070.
[25] M.P. Torres, M.P. Ponnusamy, S. Chakraborty, L.M. Smith, S. Das, H.A. Arafat, S.K. Batra, Effects of thymoquinone in the expression of mucin 4 in pancreatic cancer cells: implications for the development of novel cancer therapies, Mol. Cancer Ther. 9 (2010) 1419–1431.
[26] A.R. Hussain, M. Ahmed, S. Ahmed, P. Manogaran, L.C. Platanias, S.N. Alvi, K.S. Al-Kuraya, S. Uddin, Thymoquinone suppresses growth and induces apoptosis via generation of reactive oxygen species in primary effusion lymphoma, Free Radic. Biol. Med. 50 (2011) 978–987.
[27] W.K. Ng, L.S. Yazan, M. Ismail, Thymoquinone from *Nigella sativa* was more potent than cisplatin in eliminating of SiHa cells via apoptosis with downregulation of Bcl-2 protein, Toxicol. in Vitro 25 (2011) 1392–1398.
[28] H. Gali-Muhtasib, M. Ocker, D. Kuester, S. Krueger, Z. El-Hajj, A. Diestel, M. Evert, N. El-Najjar, B. Peters, A. Jurjus, A. Roessner, R. Schneider-Stock, Thymoquinone reduces mouse colon tumor cell invasion and inhibits tumor growth in murine colon cancer models, J. Cell. Mol. Med. 12 (2008) 330–342.
[29] T. Yi, S.G. Cho, Z. Yi, X. Pang, M. Rodriguez, Y. Wang, G. Sethi, B.B. Aggarwal, M. Liu, Thymoquinone inhibits tumor angiogenesis and tumor growth through suppressing AKT and extracellular signal-regulated kinase signaling pathways, Mol. Cancer Ther. 7 (2008) 1789–1796.
[30] A. Abusnina, M. Alhosin, T. Keravis, C.D. Muller, G. Fuhrmann, C. Bronner, C. Lugnier, Down-regulation of cyclic nucleotide phosphodiesterase PDE1A is the key event of p73 and UHRF1 deregulation in thymoquinone-induced acute lymphoblastic leukemia cell apoptosis, Cell. Signal. 23 (2011) 152–160.
[31] R.L. Gurung, S.N. Lim, A.K. Khaw, J.F. Soon, K. Shenoy, S.M. Ali, M. Jayapal, S. Sethu, R. Baskar, M.P. Hande, Thymoquinone induces telomere shortening, DNA damage and apoptosis in human glioblastoma cells, PLoS One 5 (2010) e12124.
[32] A. Arola, R. Vilar, Stabilisation of G-quadruplex DNA by small molecules, Curr. Top. Med. Chem. 8 (2008) 1405–1415.
[33] D.J. Patel, A.T. Phan, V. Kuryavyi, Human telomere, oncogenic promoter and 5′-UTR G-quadruplexes: diverse higher order DNA and RNA targets for cancer therapeutics, Nucleic Acids Res. 35 (2007) 7429–7455.
[34] E.M. Rezler, D.J. Bearss, L.H. Hurley, Telomere inhibition and telomere disruption as processes for drug targeting, Annu. Rev. Pharmacol. Toxicol. 43 (2003) 359–379.
[35] J.L. Huppert, S. Balasubramanian, G-quadruplexes in promoters throughout the human genome, Nucleic Acids Res. 35 (2007) 406–413.
[36] T.S. Dexheimer, M. Fry, L.H. Hurley, in: S. Neidle, S. Balasubramanian (Eds.), Quadruplex Nucleic Acids, Royal Society of Chemistry, UK, 2006.
[37] S. Neidle, Stephen Neidle on cancer therapy and G-quadruplex inhibitors, Drug Discov. Today 9 (2004) 778–781.
[38] H. Han, D.R. Langley, A. Rangan, L.H. Hurley, Selective interactions of cationic porphyrins with G-quadruplex structures, J. Am. Chem. Soc. 123 (2001) 8902–8913.
[39] D.P. Goncalves, R. Rodriguez, S. Balasubramanian, J.K. Sanders, Tetramethylpyridiniumporphyrazines: a new class of G-quadruplex inducing and stabilising ligands, Chem. Commun. (2006) 4685–4687.
[40] L. Ren, A. Zhang, J. Huang, P. Wang, X. Weng, L. Zhang, F. Liang, Z. Tan, X. Zhou, Quaternary ammonium zinc phthalocyanine: inhibiting telomerase by stabilizing G quadruplexes and inducing G-quadruplex structure transition and formation, Chem. BioChem. 8 (2007) 775–780.
[41] D. Seidel, V. Lynch, J.T. Sessler, Cyclo[8]pyrrole: a simple-to- make expanded porphyrin with no meso bridges, Angew. Chem. Int. 41 (2002) 1422–1425.
[42] M.Y. Kim, H. Vankayalapati, Y.K. Shin, K. Wierzba, L.H. Hurley, Telomestatin, a potent telomerase inhibitor that interacts quite specifically with the human telomeric intramolecular g-quadruplex, J. Am. Chem. Soc. 124 (2002) 2098–2099.
[43] T.Y. Mikami, M. Akiyama, Y. Yuza, T. Yanagisawa, O. Yamada, H. Yamada, Antitumor activity of G-quadruplex interactive agent TMPyP4 in K562 leukemic cells, Cancer Lett. 261 (2008) 226–234.
[44] P. Wang, L. Ren, H. He, F. Liang, X. Zhou, Z. Tan, A phenol quaternary ammonium porphyrin as a potent telomerase inhibitor by selective interaction with quadruplex DNA, Chem. BioChem. 7 (2006) 1155–1159.
[45] C. Granotier, G. Pennarun, L. Riou, F. Hoffschir, L.R. Gauthier, A. De Cian, D. Gomez, E. Mandine, J.F. Riou, J.L. Mergny, P. Mailliet, B. Dutrillaux, F.D. Boussin, Preferential binding of a G-quadruplex ligand to human chromosome ends, Nucleic Acids Res. 33 (2005) 4182–4190.
[46] L. Rossetti, M. Franceschin, S. Schirripa, A. Bianco, G. Ortaggi, M. Savino, Selective interactions of perylene derivatives having different side chains with inter- and intramolecular G-quadruplex DNA structures. A correlation with telomerase inhibition, Bioorg. Med. Chem. Lett. 15 (2005) 413–420.
[47] C. Sissi, L. Lucatello, K.A. Paul, D.J. Maloney, M.B. Boxer, M.V. Camarasa, G. Pezzoni, E. Menta, M. Palumbo, Tri-, tetra- and heptacyclic perylene analogues as new potential antineoplastic agents based on DNA telomerase inhibition, Bioorg. Med. Chem. 15 (2007) 555–562.
[48] H.M. Lee, D.S.H. Chan, F. Yang, H.Y. Lam, S.C. Yan, C.M. Che, D.L. Ma, C.H. Leung, Identification of natural product Fonsecin B as a stabilizing ligand of C-myc G-quadruplex DNA by high throughput virtual screening, Chem. Commun. 46 (2010) 4680–4682.
[49] D.S.H. Chan, H. Yang, M.H.T. Kwan, Z. Cheng, P. Lee, L.P. Bai, Z.H. Jiang, C.Y. Wong, W.F. Fong, C.H. Leung, D.L. Ma, Structure-based optimization of FDA-approved drug methylene blue as a c-myc G-quadruplex DNA stabilizer, Biochimie 93 (2011) 1055–1064.
[50] J.E. Reed, A.A. Arnal, S. Neidle, R. Vilar, Stabilization of G-quadruplex DNA and inhibition of telomerase activity by square planar nickel(II) complexes, J. Am. Chem. Soc. 128 (2006) 5992–5993.
[51] J.E. Reed, S. Neidle, R. Vilar, Stabilisation of human telomeric quadruplex DNA and inhibition of telomerase by a platinum phenanthroline complex, Chem. Commun. (2007) 4366–4368.
[52] D.L. Ma, C.M. Che, S.C. Yan, Platinium (II) complexes with dipyridophenazine ligands as human telomerase inhibitors and luminescent probes for G-quadruplex DNA, J. Am. Chem. Soc. 131 (5) (2009) 1835–1846 (11).
[53] H.Z. He, K.H. Leung, W. Wang, D.S.H. Chan, C.H. Leung, D.L. Ma, Label-free luminescence switch-on detection of T4 polynucleotide kinase activity using G-quadruplex-selective probe, Chem. Commun. 50 (2014) 5313 (and references cited there in).
[54] H. Bertrand, D. Monchaud, A. De Cian, R. Guillot, J.L. Mergny, F.M.P. Teulade, The importance of metal geometry in the recognition of G-quadruplex-DNA by metal-terpyridine complexes, Org. Biomol. Chem. 5 (2007) 2555–2559.
[55] B.B. Aggarwal, A.B. Kunnumakkara, K.B. Harikumar, S.T. Tharakan, B. Sung, P. Anand, Potential of spice-derived phytochemicals for cancer prevention, Planta Med. 74 (2008) 1560–1569.
[56] K. Wu, J. Fei, W. Bai, S. Hu, Direct electrochemistry of DNA guanine and adenine at a nanostructured film-modified electrode, Anal. Bioanal. Chem. 376 (2003) 205–209.
[57] J.B. Conant, L.F. Fieser, Reduction potentials of quinones I. The effect of the solvent on the potentials of certain benzoquinones, J. Am. Chem. Soc. 45 (9) (1923) 2194–2218.
[58] G. Bonner, A.M. Klibanov, Structural stability of DNA in nonaqueous solvents, Biotechnol. Bioeng. 68 (3) (2000) 339–344.
[59] C.M. Orlando, H. Mark, A.K. Bose, M.S. Manhas, Photoreactions. V. Mechanism of the photo rearrangement of alkyl-*p*-benzoquinones, J. Org. Chem. 55 (6) (1968) 2512–2516 (Also see Kuboyama, A. The very weak visible absorption band of p-benzoquinone. Bull. Chem. Soc. Jap. 1962, 35 (2), 295–298).
[60] H.W. Moore, Mono- and diepoxy-1,4-benzoquinones, J. Am. Chem. Soc. 32 (1967) 1996–1999.
[61] Y. Xu, Y. Noguchi, H. Sugiyama, The new models of the human telomere d [AGGG(TTAGGG)$_3$] in K^+ solution, Bioorg. Med. Chem. 14 (2006) 5584–5591.
[62] A. Ambrus, D. Chen, J. Dai, T. Bialis, R.A. Jones, D. Yang, Human telomeric sequence forms a hybrid-type intramolecular G-quadruplex structure with mixed parallel/antiparallel strands in potassium solution, Nucleic Acids Res. 34 (9) (2006) 2723–2735.
[63] J. Tan, L. Gu, J. Wu, Design of selective G-quadruplex ligands as potential anticancer agents, Mini-Rev. Med. Chem. 8 (2008) 1163–1178.
[64] J. Dash, R.N. Das, N. Hegde, G.D. Pantos, P.S. Shirude, S. Balasubramanian, Synthesis of bis-indole carboxamides as G-quadruplex stabilizing and inducing ligands, Chem. Eur. J. 18 (2012) 554–564.
[65] Y. Du, D. Zhang, W. Chen, M. Zhang, Y. Zhou, X. Zhou, Cationic N-confused porphyrin derivative as a better molecule scaffold for G-quadruplex recognition, Bioorg. Med. Chem. 18 (2010) 1111–1116.
[66] J.D. McGhee, P.H. von Hippel, Theoretical aspects of DNA-protein interactions: co-operative and non-co-operative binding of large ligands to a one-dimensional homogeneous lattice, J. Mol. Biol. 86 (2) (1974) 469–489.

[67] D. Khananshvili, Z.G. Elhanan, Demonstration of two binding sites for ADP on the isolated β-subunit of the *Rhodospirillum rubrum* R1FoF1-ATP synthase, FEBS 178 (1) (1984) 10–14.
[68] C. Wei, G. Jia, J. Yuan, Z. Feng, A.C. Li, Spectroscopic study on the interactions of porphyrin with G-quadruplex DNAs, Biochemistry 45 (2006) 6681–6691.
[69] D. Harvey, Modern Analytical Chemistry, McGraw Hill, Higher Education, 2000. 40.
[70] E.A. Boudreau, I. Pelczer, P.N. Borer, G.J. Heffron, S.R. LaPlante, Changes in drug ^{13}C NMR chemical shifts as a tool for monitoring interactions with DNA, Biophys. Chem. 109 (2004) 333–344.
[71] Z.A.E. Walter, S.A. Sewitz, S.D. Hsu, S. Balasubramanian, A small molecule that disrupts G-quadruplex DNA structure and enhances gene expression, J. Am. Chem. Soc. 131 (2009) 12628–12633.
[72] P. Tang, R.A. Santos, G.S. Harbison, Two-dimensional solid-state nuclear magnetic resonance studies of the conformation of oriented DNA, Adv. Magn. Reson. 13 (1989) 225–255.
[73] S.R. LaPlantea, P.N. Borer, Changes in ^{13}C NMR chemical shifts of DNA as a tool for monitoring drug interactions, Biophys. Chem. 90 (2001) 219–232.
[74] Y. Ma, T.M. Ou, J.H. Tan, J.Q. Hou, S.L. Huang, L.Q. Gu, Z.S. Huang, Synthesis and evaluation of 9-O-substituted berberine derivatives containing aza-aromatic terminal group as highly selective telomeric G-quadruplex stabilizing ligands, Bioorg. Med. Chem. Lett. 19 (2009) 3414–3417.
[75] H. Simpkins, L.F. Peariman, L.M. Thompson, Effects of adriamycin on supercoiled DNA and calf thymus nucleosomes studied with fluorescent probes, Cancer Res. 44 (1984) 613–618.
[76] G. Lenglet, M.D. Cordonnier, DNA destabilizing agents as an alternative approach for targeting DNA: mechanisms of action and cellular consequences, J. Nucleic Acids (2010) 1–17 (article ID # 290935).
[77] C. Zhao, J. Ren, J. Gregolinski, J. Lisowski, X. Qu, Contrasting enantioselective DNA preference: chiral helical macrocyclic lanthanide complex binding to DNA, Nucleic Acids Res. 40 (16) (2012) 8186–8196.
[78] S.R. Brozell, S. Mukherjee, T.E. Balius, D.R. Roe, D.A. Case, R.C. Rizzo, Evaluation of DOCK 6 as a pose generation and database enrichment tool, J. Comput. Aided Mol. Des. 26 (6) (2012) 749–773.
[79] Discovery Studio Modeling Environment, Release 3.5, Accelrys Software Inc., San Diego, 2012.
[80] F.S. Di Leva, E. Novellino, A. Cavalli, M. Parrinello, V. Limongelli, Mechanistic insight into ligand binding to G-quadruplex DNA, Nucleic Acids Res. 42 (9) (2014) 5447–5455.